PROCEEDINGS, 51st Workshop on Geothermal Reservoir Engineering
Stanford University, Stanford, California, February 9-11, 2026
SGP-TR-230

Tracer Testing in Propped EGS Fractures: Modeling and Analysis

Sarah Sausan, Roland Horne

Stanford Geothermal Program at Energy Science & Engineering Department, Stanford University

sausan@stanford.edu

Keywords: Flowthrough tracer, stim tracer, EGS, nanotracers, chemical tracers, conservative tracers

ABSTRACT

This paper details the modeling and analysis tracer testing in propped EGS fractures using Utah FORGE tracer data. Two types of tracer tests were conducted at Utah FORGE: stim tracer testing, performed during stimulation with stage-unique tracers mixed with proppant, and flowthrough tracer testing deployed during crossflow and circulation tests. Stim tracer results obtained in 2024, deployed using different compositions (nano- versus chemical tracers) and methodologies, were compared to inform the stim tracer deployment strategy in propped EGS fields. Additionally, a methodology for modeling multicomponent flowthrough tracers in EGS wells is being developed.

The stim tracer analysis encompasses various deployment and sampling strategies, including the use of chemical versus nanotracers, different sampling durations, and sampling frequencies. Stim tracer results were analyzed for concentration trends, flow contributions, and tracer recovery returns. Our analysis shows that simultaneously deploying both nano- and chemical stim tracers helped compare their behavior and effectiveness, as well as establishing a baseline for subsequent analyses, especially given that the nanotracer dataset has consistently shown more erratic patterns than chemical tracers.

The multicomponent tracer model employs tracer dispersion as the governing equation and least-squares fitting with a soft flow-fraction penalty as the objective function. Synthetic datasets were generated to aid in model development. This initial attempt at multicomponent tracer modeling in EGS wells demonstrated promising results, especially when involving a few components. Improvements to the modeling techniques will be explored to enable the model to better handle a larger number of components.

1. INTRODUCTION

Commercial breakthroughs in Enhanced Geothermal Systems (EGS) have been achieved through proppant-based stimulation techniques. Still, systemic characterization of propped fractures for geothermal applications remains in early stages, particularly regarding heat transfer efficiency, circulation dynamics, and short-circuiting risk. Field-wide characterization methodologies, especially tracer testing, offer promising approaches to infer connectivity patterns, fracture productivity, and heat-transfer capabilities within proppant-assisted reservoirs.

Tracer testing involves injecting a tracer-carrying fluid into the reservoir interval(s) and subsequently monitoring the tracer concentration from producing wells. For propped EGS, two types of tracer testing have been deployed: (a) stim tracers, in which stimulation stages are tagged with unique tracer fluid species mixed with proppant and recovered during flowback and/or circulation tests, and (b) flowthrough tracers, in which tracers are injected at injection well(s) during circulation tests and sampled at other wells, usually producers. Stim tracer testing for propped EGS has been adapted from unconventional oil and gas (i.e., "shale"), whereas flow-through tracer deployment is a standard practice in conventional geothermal systems. However, the unique objectives for propped EGS and conditions warrant re-examining the procedures and analysis techniques previously developed for the original systems (Figure 1). For example, shale systems mainly consist of production wells spaced closely together but which are not intended to interact, in order to optimize hydrocarbon output while avoiding "frac hits". Thus, in oil and gas applications the stim tracer test is deployed during stimulations to identify frac-hit-inducing stages in nearby production wells. Additionally, circulation testing, or crossflow, is uncommon in shale; hence, the practice of recovering proppant-mixed stim tracer samples from offset wells is unique to propped EGS (stim tracers in shale applications are usually recovered via flowback).

Similarly, flowthrough tracer testing has been routinely deployed in conventional geothermal systems to infer flow path and to derive reservoir productivity indicators. However, conventional systems typically involve only a few feed zones with well placements spaced far apart to minimize the risk of interference, especially early in field development. In contrast, propped EGS settings, as demonstrated at Cape Station, consist of closely spaced long laterals with a large number of stages (Fercho et al., 2025; Singh et al., 2025; Kim et al., 2026). While deployment and sampling methods between conventional geothermal and propped EGS may be similar, the assumptions underlying tracer return curve analysis may differ due to the proximity of producer and injector pairs and the much larger number of feed zones involved.

In this paper, the examination of the tracer test procedure and analysis focused on the dataset collected at the Utah FORGE site in 2024. The first section of this paper compares stim tracer results obtained by different service providers and methodologies to provide insights into the stim tracer deployment strategy in propped EGS wells. The second section details the development of a methodology for modeling

multicomponent flow-through tracers in EGS wells, which have many more stages than traditional geothermal wells with only a few feed zones.

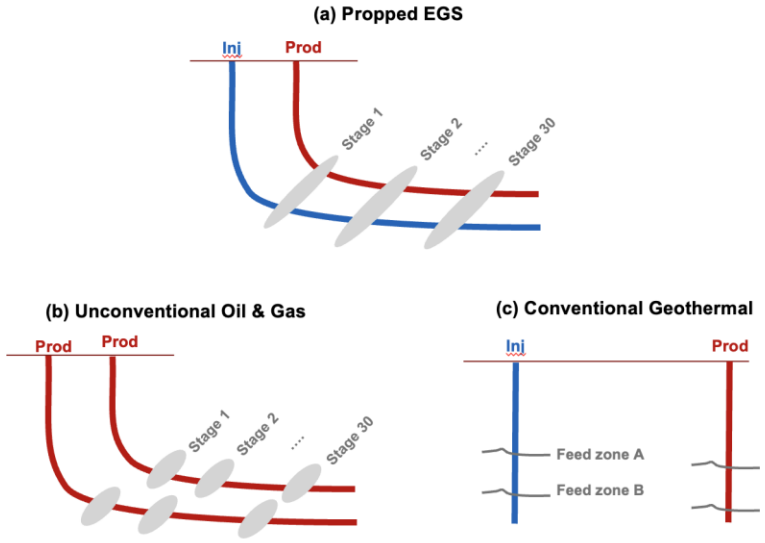

Figure 1: Illustration of different doublet well configurations that affect assumptions made during the tracer testing procedure and analysis in (a) propped EGS, (b) unconventional oil & gas, i.e., shale, and (c) conventional geothermal systems.

2. STIM TRACER ANALYSIS

2.1 Overview

In this study, stim tracer analysis was focused on the stim tracer datasets collected in between April and September 2024 at the Utah FORGE site. Stim tracer results were analyzed for concentration trends, flow contributions, and tracer recovery returns plotted versus time and/or cumulative produced volume. The stim tracer tests were performed using nanotracers from QuantumPro and chemical tracers from RESMAN. Tracers from each vendor were deployed at each stage during stimulation of well 16A(78)-32 (abbreviated as 16A) in early April. A series of sampling periods followed, which included the 16A flowback after stimulation, sampling at 16A(78)-32 (abbreviated as 16B) during a 9-hour circulation on April 27, 2024, and 16B sampling during the 1-month extended circulation test conducted between August and September 2024.

QuantumPro's FloTrac nanotracers are stated by QuantumPro Inc (2025) to be water and oil-compatible, thermally stable up to 2,000°F (1,093°C), and inert, with particle sizes much smaller than frac sand particles (Figure 2). Meanwhile, the RESMAN chemical tracers deployed at Utah FORGE are conservative, water-soluble chemical tracers of naphthalene disulfonate (NDS) and IFE variety; the latter is of proprietary chemistry but appears to be based on fluorinated benzoic acids (Hartvig, n.d.). RESMAN tracers are also stated to be inert and to have passed thermal stability testing under Utah FORGE conditions of up to 464°F or 240°C (Fredd et al., 2025a; Fredd et al., 2025b).

Figure 2: Comparison of FloTrac tracer particle size with different types of proppant sand (Guo et al., 2025)

Stim tracer results were analyzed for concentration trends, flow contributions, and cumulative tracer recovery. The plots are shown as a function of the cumulative produced volume. For the extended circulation test period, the produced volume was derived from the 16B total separator rate, corrected for the steam fraction calculated at each data point using the flash correction factor (FCF) of the atmospheric separator method, as described by Grant and Bixley (2022). This rate correction is necessary because the sampling location precedes the separator, whereas the reliable rate sensor is located downstream of the separator. The flowback data period lacks a reliable discharge rate

of 16A; thus, the cumulative produced volume was derived from RESMAN-logged production volume data and corrected using a steam fraction of 19.6%, as reported in McLennan et al. (2024). The sampling location varies, particularly at the start of flowback, so circulation test data are generally sampled more consistently and are supported by more reliable rate data.

2.2 Concentration Trends

Figure 3 shows the stim tracer concentration trend throughout the sampling period at Utah FORGE, including 16A flowback on 7-22 April 2024, a 9-hour circulation test on April 27, 2024, and the extended circulation test in August-September 2024. The plots show distinct trends; the chemical tracer data are quite erratic during 16A flowback but gradually stabilize, especially during the circulation test. In contrast, the nanotracers dataset exhibits considerable variation well into the extended circulation period.

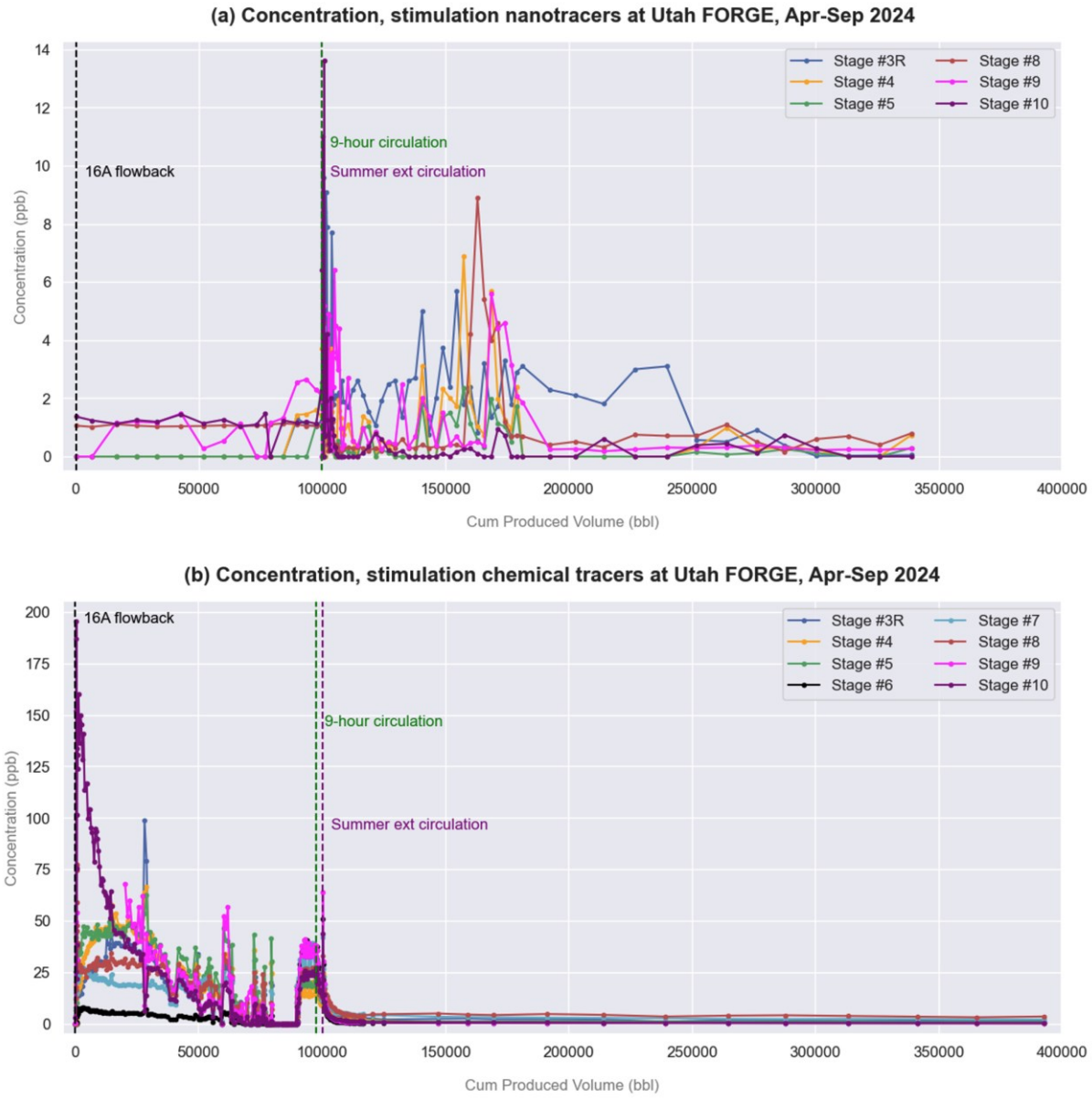

Figure 3: Utah FORGE stim tracer concentration trend using (a) nanotracers and (b) chemical tracers, from April to September 2024, combining three datasets: 16A flowback (April 7-22), 9-hour circulation test (April 27), and extended circulation test (August-September).

In terms of sampling frequency, the chemical tracers were sampled multiple times a day during the 16A flowback, whereas the nanotracer data was sampled once a day. During the 9-hour circulation, the nanotracers were sampled only once, whereas the chemical tracers were sampled every 20 minutes. Meanwhile, during the extended circulation test, both the nanotracers and chemical tracers were sampled more frequently at the beginning, approximately every 30 minutes to 1.5 hours, then reduced to twice a day, which is a standard practice for tracer sampling.

During the 16A flowback period, although the chemical tracer concentration decreased, the nanotracer data do not exhibit a similar trend. Additionally, nanotracer returns were not observed during flowback but reappeared either very late into the flowback, as seen in Stage 4, or during the following circulation test, as in Stage 3R. Guo et al (2025) related the presence of certain stages during flowback with the timing of frac plug drill-out. Fredd et al. (2025a) noted that the chemical tracer 16A flowback data were affected by changes in sampling locations and frequent field operations, which contributed to concentration variation during the period.

Concentration trends from the nanotracer datasets during circulation tests (Figure 4) show that in the chemical tracer circulation test dataset, the concentration initially peaks, then peaks again roughly a third of the way through the extended circulation test. Meanwhile, the water-soluble chemical tracers showed an early peak, followed by a rapid decline and then a plateau. The second concentration peak observed with the nanotracers was not replicated by the chemical tracers. In stim tracer returns, the apparent peaks observed in both nanotracers and chemical tracers are attributed to disturbances caused by surface or downhole field activities, unlike the peaks in flowthrough tracer returns, which can serve as valuable indicators of flow paths when modeled. However, it is interesting to note that while the circulation startup peaks are present for both chemical and nanotracer samples, the peak midway through the circulation test is unique to the nanotracer return. This peak is examined further during the tracer cumulative recovery discussion in Section 2.4.

Additionally, adding a flowthrough tracer injection can help determine the first temporal moment shortly after stimulation, which is useful even for a brief crossflow, such as the 9-hour circulation test. During the April 2024 9-hour circulation, a flowthrough chemical tracer was injected, shown as a black line in Figure 4b. A similar flowthrough injection during the 9-hour circulation test was not performed with the nanotracers.

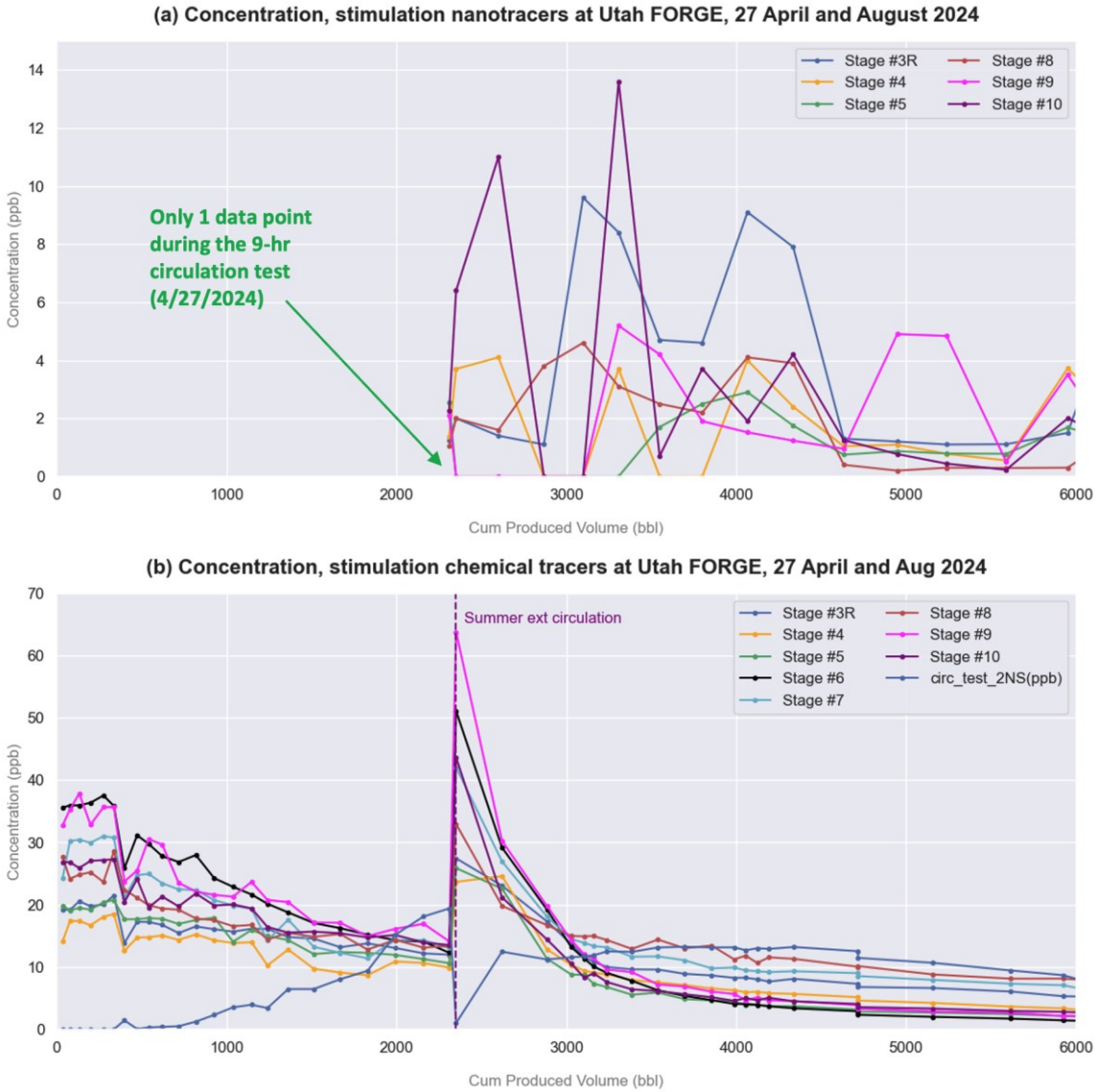

Figure 4: Circulation test subset of Utah FORGE stim tracer concentration trend using (a) nanotracers and (b) chemical tracers. Data is compiled from the 27 April 9-hour circulation test, and the start of the August-September extended circulation test in 2024. The produced volume horizontal axis is reset at the start of the 9-hour circulation test data.

2.3 Flow Contribution and Ranking

Flow contribution is the ratio of the concentration from each stage to the total concentration recorded at each sampling period (Eq. 1). This parameter helps evaluate stimulation effectiveness, such as identifying whether different stimulation strategies lead to more productive stages. Additionally, a discrete ranking was created alongside the flow contribution plots to aid analysis. For propped-fracture EGS with relatively uniform stimulation design across stages, it is desired that the flow contribution among stages be as uniform as possible to minimize the dominance of certain stages and thus prevent premature cooling.

$$\text{Flow contribution } (\%) = \frac{c_{\text{stage}}}{c_{\text{total}}} \times 100\% \quad \text{(Eq. 1)}$$

Figure 5 and 6 show the flow contribution and ranking plots, respectively, throughout the sampling period at Utah FORGE, including 16A flowback on 7-22 April 2024, a 9-hour circulation test on April 27, 2024, and the extended circulation test in August-September 2024. As previously observed in the concentration trends, the chemical tracer dataset shows high variation in contribution ranking during 16A flowback but stabilizes during the circulation test. The nanotracer dataset did not capture certain stages during 16A flowback, which Guo et al (2025) stated are related to frac plug drillout timing; these stages are missing from the flow contribution ranking chart but reappeared during the circulation test.

The variability in flow contribution ranking on the nanotracer dataset is higher than in the chemical tracer dataset. The maximum flow contribution can reach 80% for nanotracers and 40% for chemical tracers. Table 1 displays the uniformity metrics across datasets, specifically the standard deviation and the coefficient of variation. Both metrics double when switching from chemical to nanotracers.

Table 1: Uniformity measures of flow contribution from different datasets, averaged over ranges

	Full Range		16A flowback		Circulation Test	
	Standard Deviation	Coefficient of Variation (%)	Standard Deviation	Coefficient of Variation (%)	Standard Deviation	Coefficient of Variation (%)
Utah FORGE, chemical tracers	8.76	67.77	9.79	74.96	7.91	63.29
Utah FORGE, nanotracers	19.06	114.38	19.42	116.49	19.18	115.07

Paired with the ranking plot (Figure 6), the varying natural conditions and the different stimulation strategies employed can explain the Utah FORGE results. For instance, Stage 8 contains the highest natural fracture intensity and was also injected with the largest proppant mass and treatment volume. The chemical tracer data show that Stage 8 contributed to the flow fairly consistently throughout the combined sampling period (short and extended circulation tests). However, the flow contribution and ranking trends of the nanotracer data are less clear. Stage 8 dominated towards the end of the sampling period, while earlier, Stage 3R was more prominent, although the ranking often changed between sampling periods (Figure 6b). Stage 3R is shown as the second most prominent contributor in the chemical tracer data and thus is not substantially different from the nanotracer data; however, the lack of consistency in the temporal ranking of the nanotracer data is worth noting.

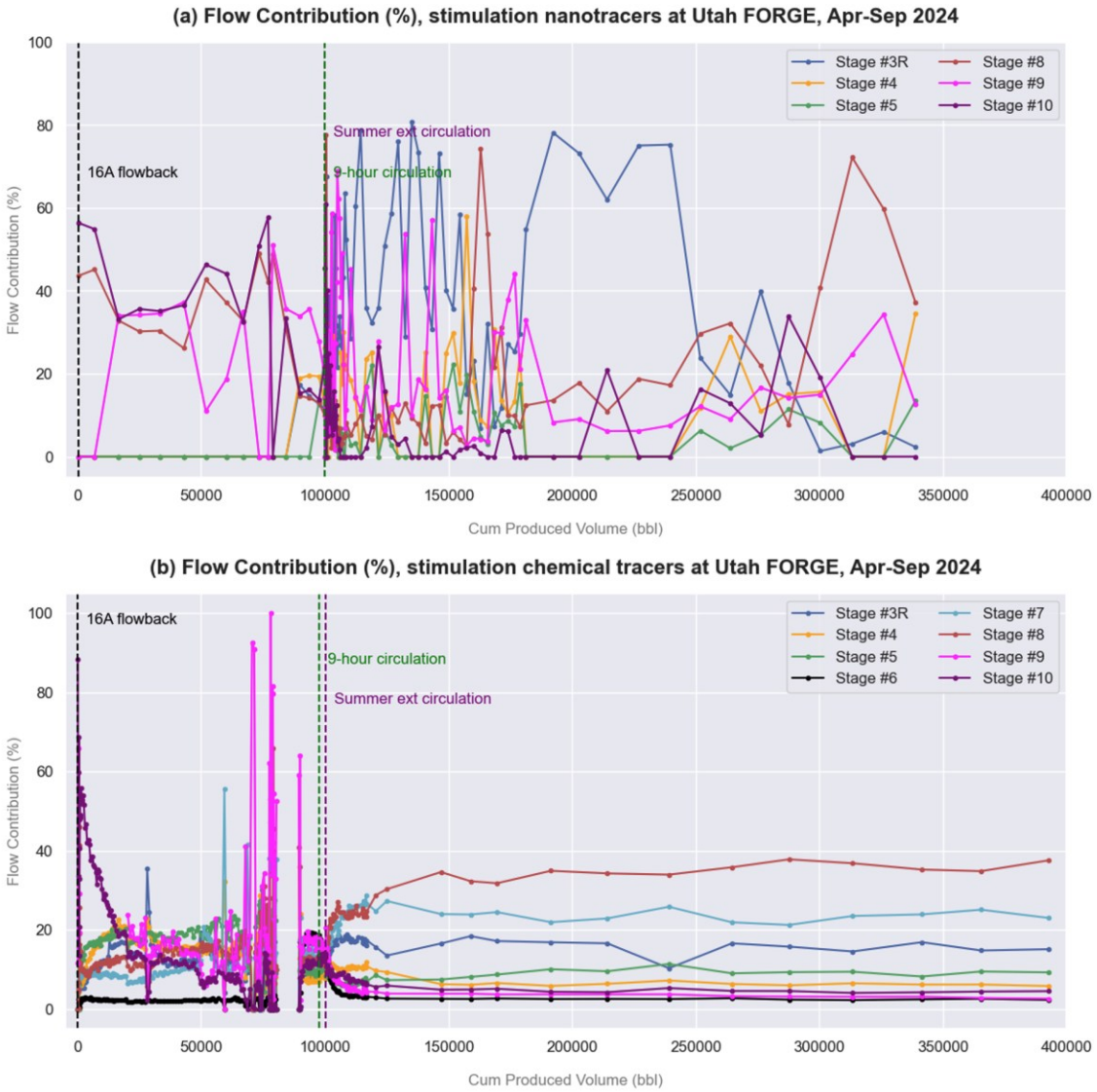

Figure 5: Flow contribution of using (a) nanotracers and (b) chemical tracersstim tracers in 2024, combining three datasets: 16A flowback (April 7-22), 9-hour circulation test (April 27), and extended circulation test (August-September).

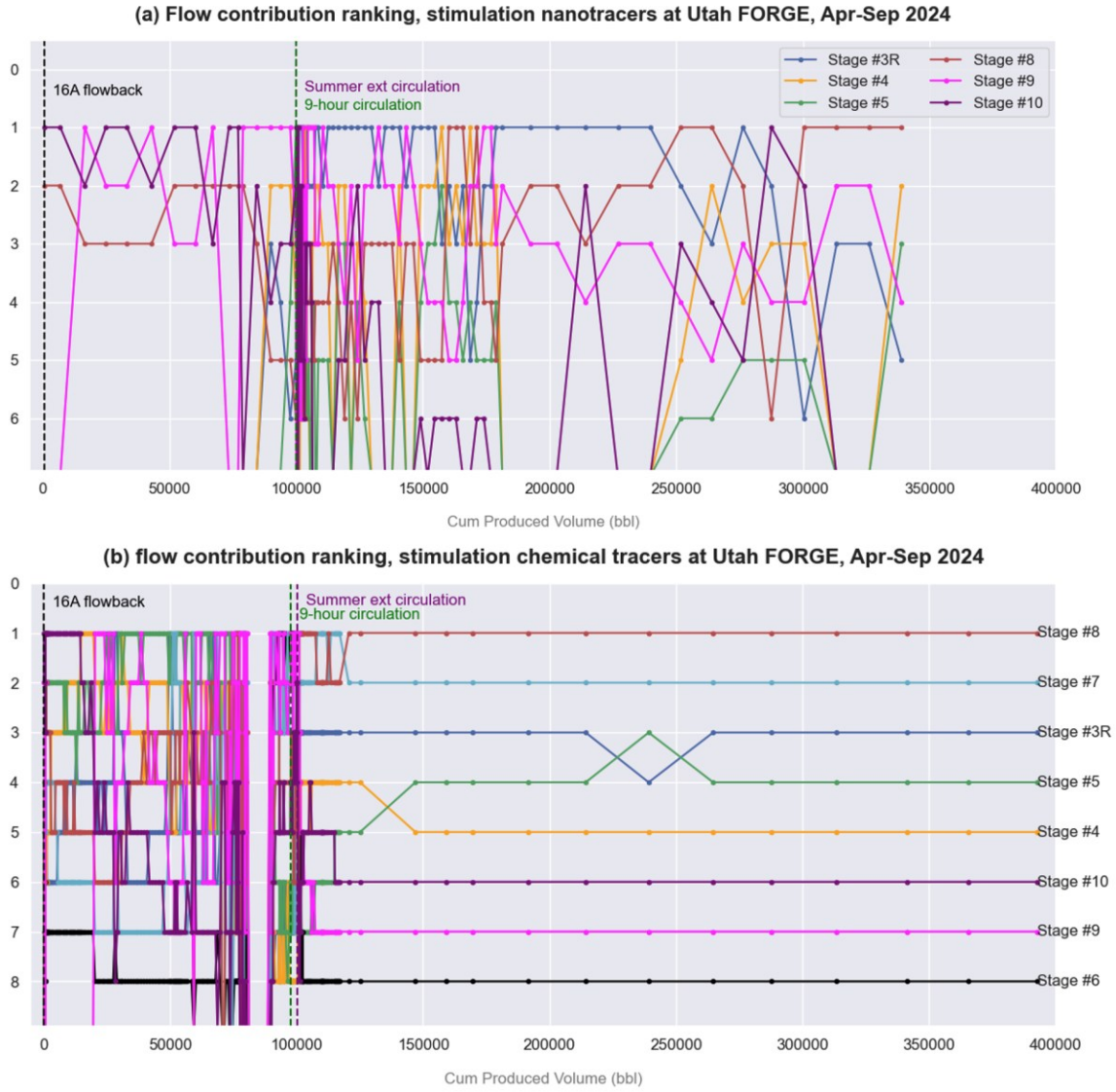

Figure 6: Flow contribution ranking of stim tracers using (a) nanotracers and (b) chemical tracers combining three datasets: 16A flowback (April 7-22), 9-hour circulation test (April 27), and extended circulation test (August-September).

2.4 Cumulative Tracer Recovery

Cumulative tracer recovery shows the cumulative mass return over the sampling period (Eq. 2). Tracer recovery returns are also normalized by the injected tracer mass (i.e., fractional recovery), using the provided injected mass data for the chemical tracer dataset (Hartvig et al., 2025). The nanotracer dataset (Guo et al., 2025) did not include injected mass. However, personal communications and deployment details from de Melo et al. (2024) suggest a standard procedure of injecting 7 lb of mass per stage at 15.5 ppm, delivered at a uniform rate without pulsing. This information was used to estimate the injected mass for normalizing the nanotracer dataset.

$$\text{Tracer recovery between two samplings (g)} = \frac{(c_2 + c_1)}{2} \cdot q \cdot \Delta t \qquad \text{(Eq. 2)}$$

Figure 7 (a) and (b) shows the normalized cumulative tracer recovery throughout the sampling period at Utah FORGE, including 16A flowback on 7-22 April 2024, a 9-hour circulation test on April 27, 2024, and the extended circulation test in August-September 2024. The 30-day sampling period during the extended circulation test at Utah FORGE allows us to observe a pattern of cumulative tracer recovery: an initial recovery jump at the start of the extended circulation test, followed by a linear trend, and finally a plateau. This pattern is especially evident in the nanotracer data. The plateau arrival time varied and could take up to two weeks after the initial sampling, as observed in stage 3R of the nanotracer data.

The nanotracer profile in Figure 8 is particularly noteworthy because some stages show a sudden tracer recovery jump, appearing as an anomalous slope between August 15 and 19. By examining the start and end times of these anomalous slopes at Stages 4, 5, 8, and 9 (Figure 9), and comparing them with the field daily report and instrumentation data. It can be inferred that some of the later disturbances

are linked to increased field activities on August 17 to 19, such as pumping shutdowns and PLT logging. However, the earlier disturbances related to the start of the slope did not match any field activity, which remained quiet on August 15 and 16 according to the field daily reports (Swearingen, 2024). Importantly, the anomalous slope behavior was not reflected in the chemical tracer data, suggesting it may be a phenomenon specific to nanotracer physical properties that can produce anomalous returns unrelated to actual fluid flow. Coincidentally, the USGS earthquake catalog shows a 3.3 Magnitude earthquake around 130 km southeast of the Utah FORGE site at the start of the disturbance (August 15, 2024, at 12 pm MST); however the activity was not picked up by the local geophone onsite. Thus, the cause of the disturbance trigger remains inconclusive.

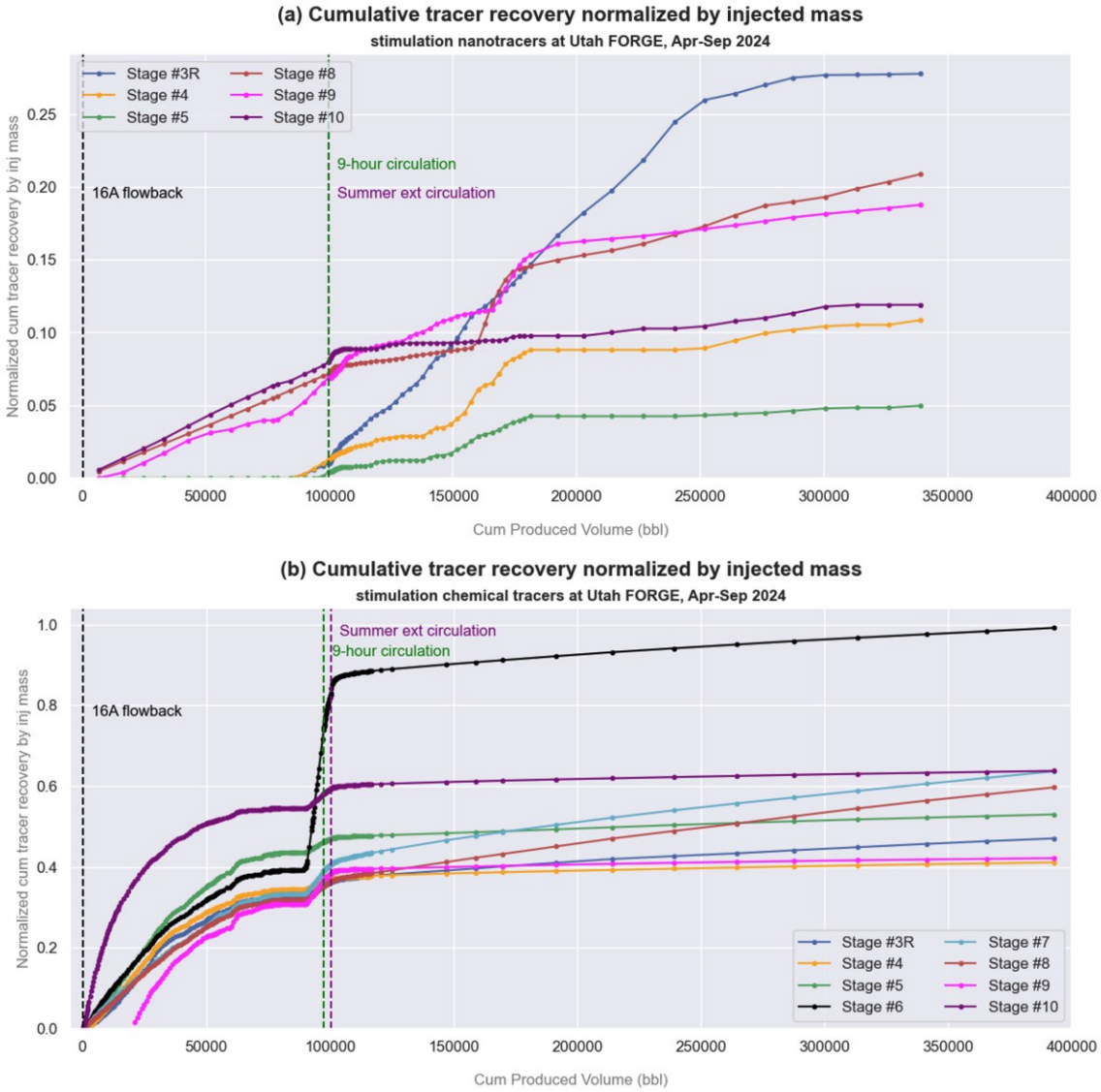

Figure 7: Cumulative tracer recovery normalized by injection mass using (a) nanotracers and (b) chemical tracers from April to September 2024, combining three datasets: 16A flowback (April 7-22), 9-hour circulation test (April 27), and extended circulation test (August-September).

Figure 8: Comparison of normalized cumulative tracer recovery for stim tracers using nanotracers and chemical tracers during the extended circulation test at Utah FORGE, August-September 2024. Cumulative produced volume is on the horizontal axis and resets since the start of the extended circulation test.

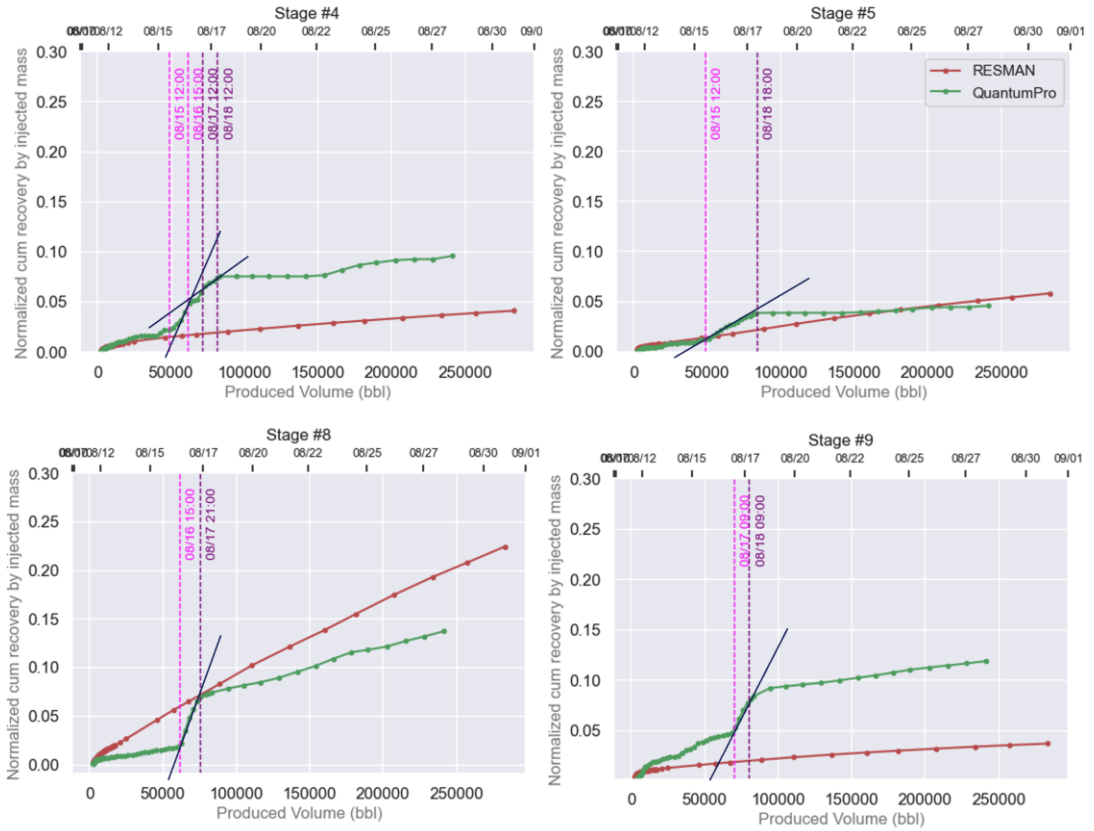

Figure 9: Start and end times of the anomalous slopes (magenta and purple dashed lines, respectively) are denoted at each stage. The produced volume on the horizontal axis is reset from the start of the circulation test.

3. FLOWTHROUGH TRACER MODELING

For flowthrough tracer analysis, we are developing multicomponent modeling methodology to separate the composite signals from the fracture stages that constitute the flow-through tracer test data. Our tracer return modeling employed the fracture model of tracer dispersion as shown in (Eq. 3) and (Eq. 4):

$$C(t) = \frac{s}{2}\sqrt{\frac{\mathrm{Pe}\,t_c}{\pi\,t}}\,\exp\!\left(-\frac{\mathrm{Pe}\,(t-t_c)^2}{4\,t\,t_c}\right) \quad \text{(Eq. 3)}$$

$$\mathrm{Pe} = \frac{u\,x}{\eta} \quad \text{(Eq. 4)}$$

When using dataset obtained from crossflow or circulation test, injection recycling corrections needs to be performed by applying the analytical solution from Grant & Bixley (2011), modified from Shook (2005) as shown in (Eq. 5). To account for the contribution of the two injection wells, the rates of 3-I and 1-I were summed to obtain the injection flow rate.

$$c_i(t) \;=\; c_i'(t) \;-\; \frac{1}{M}\int_{t_1}^{t} c_i(t-\tau)\,c_I(\tau)\,W_I(\tau)\,d\tau \quad \text{(Eq. 5)}$$

To assist with the model development, a synthetic tracer return dataset was generated for testing purposes. Additionally, a matching algorithm was developed to evaluate the closeness of the predicted component vs. the ground truth quantitatively.

3.1 Dataset generation and component matching evaluation

For testing purposes, a synthetic dataset was generated by varying the parameter values for $\underline{s}$, u, and η of Equations (2) and (3). The parameter s represents the mass of tracer injected and has a linear effect on the model, whereas u and η have a nonlinear contribution to the resulting tracer return. The synthetic dataset was generated by first sampling 5,000 parameter values for s, u, and η from their constrained ranges, centered on the single-component fitting parameter values fitted to a propped-fracture EGS field tracer returns. Then, 500 parameter combinations were drawn from these 5,000 parameter sets to generate the composite tracer return for k parameters, with k also randomized within a specified range. Finally, Gaussian noise was added to the generated data to simulate natural variation. Visual sanity checks also informed the range width: cases in which the resulting composite return signal increases with time do not reflect the typical profile of a tracer return; thus, the range width was adjusted accordingly to minimize such cases.

A component similarity evaluation algorithm was developed to identify the best match between each predicted component of a tracer signal and its corresponding ground-truth component. The linear sum assignment algorithm, also known as the Hungarian algorithm, was employed for this purpose as shown in (Eq. 6). The algorithm is an objective function that minimizes the matching cost, defined as the relative L2 norm (Eq. 7), over all possible combinations of components.

$$\min \sum_i \sum_j C_{i,j} X_{i,j} \quad \text{(Eq. 6)}$$

$$\text{Relative L2} = \frac{||\mathbf{y}_{true} - \mathbf{y}_{pred}||_2}{||\mathbf{y}_{true}||_2} \quad \text{(Eq. 7)}$$

3.2 Least-square fitting

The single-component model was fitted by minimizing the sum of least-squares error between the data and model curves; it was therefore natural to extend this approach to develop the multicomponent model. The multicomponent fitting seeks the combination of fitting parameters $\underline{s_1}$, u_1, η_1, ..., $\underline{s_k}$, u_k, η_k that minimizes the objective function (Eq. 8), where the first term represents the conventional least-squares minimization of the distance between the observed and true concentrations of the sum of components.

The second term is a soft penalty term from an additional input parameter *s_frac,* or fractions of $s_1, \ldots s_k$ from the components. The *s_frac* can be determined in advance by relating it to the flow contribution of each stage, as inferred from spinner logs or stim tracers. The weight parameter W adjusts the penalty strength; testing varying W shows that increasing W yields diminishing returns in error reduction. An overly strong penalty will make it difficult for the model to identify permissible parameter combinations and thus increase the error. Generally, keeping W=1 appears sufficient to benefit from *s_frac* guidance.

$$\min_{\mathbf{p}} \left(\underbrace{\sum_t \left(C_{pred}(t,\mathbf{p}) - C_{obs}(t)\right)^2}_{\text{Concentration diff term (main target)}} + \underbrace{\sum_k \left(\left(\frac{s_k}{\sum_j s_j} - f_{target,k} \right) \cdot W \cdot \max(C_{obs}) \right)^2}_{\text{s\_frac penalty term}} \right) \quad \text{(Eq. 8)}$$

We started the multicomponent model testing with a three-component tracer return signal (i.e., k = 3) using the synthetic dataset as shown in Figure 10(a). Compared to the single-component fitting of the same dataset (Figure 10b), the multicomponent fitting delivered 80.67% smaller least-square error. Furthermore, when the fraction of s parameter *s_frac* was given as an additional input, the fitting yielded 91.73% smaller least-square error. Interestingly, the matching algorithm yields different results with or without the *s_frac* input (Figure

11), with the minimized matching costs decreasing from 1.72 to 1.17. This result demonstrated the superiority of multicomponent fitting with *s_frac* input, when applicable.

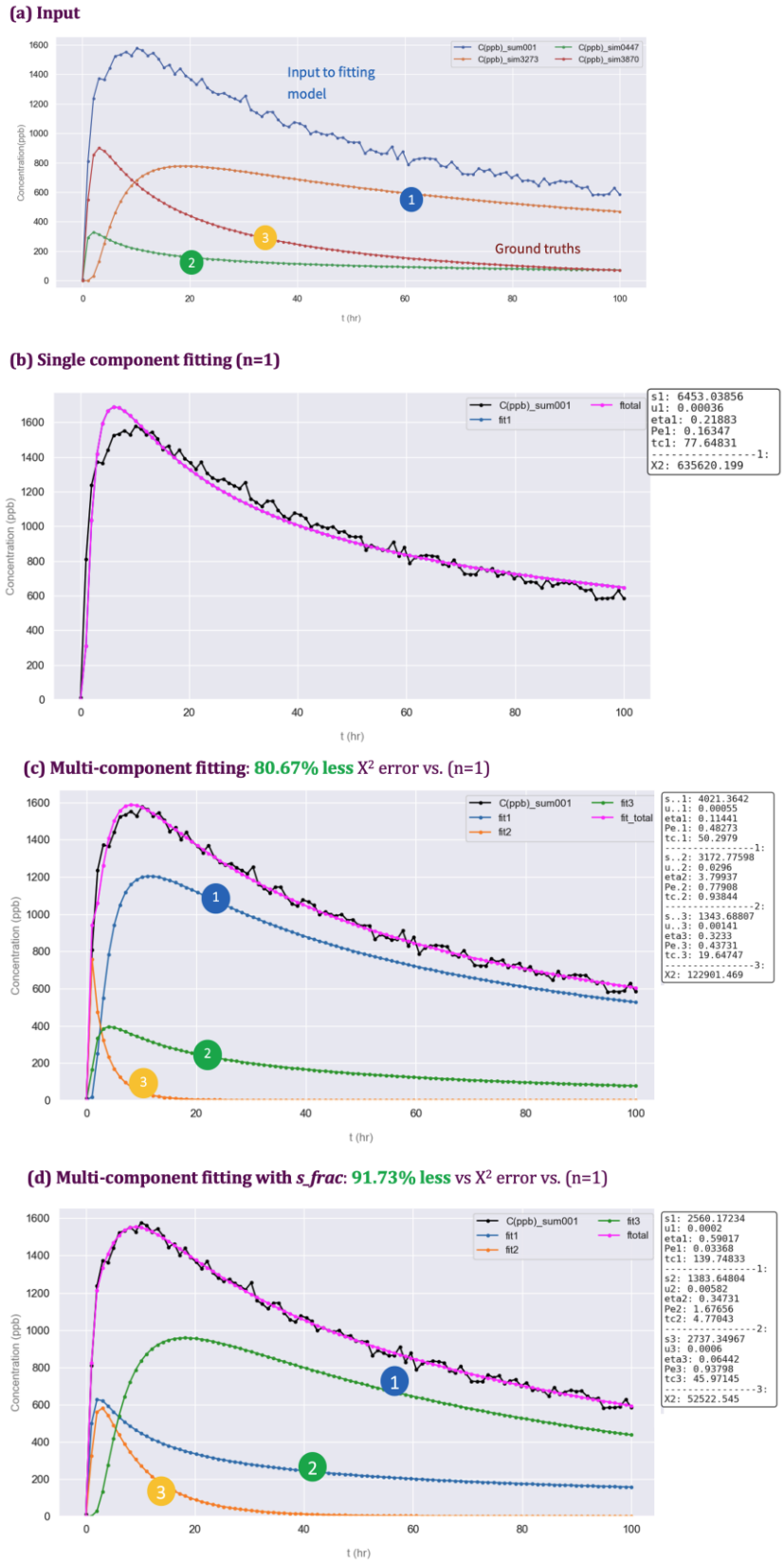

Figure 10: (a) Synthetic dataset used to develop the multi-k least-square fitting method with k = 3; results of (b) single-component fitting, (c) multicomponent fitting, and (d) multicomponent fitting with additional parameter *s_frac*.

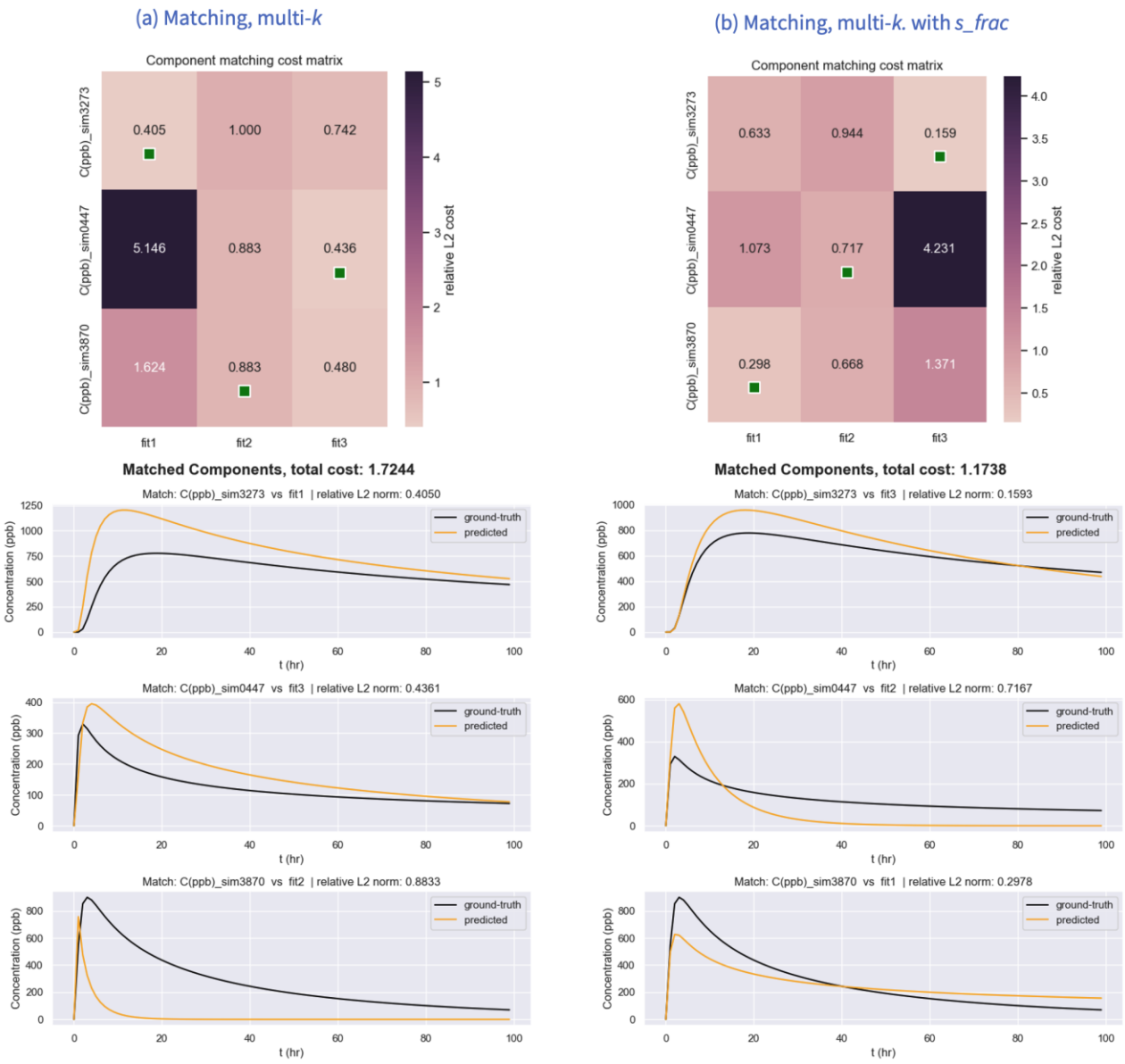

Figure 11: algorithmic matching results for multicomponent fitting (a) without and (b) with *s_frac*.

Although the three-component model was successful, we wanted to examine whether this success extends to a larger number of components, such as $k = 30$. The model requires fitting 3 x k parameters, so a larger k will pose challenges for least-squares fitting. One remediation strategy may be to improve the initial parameter estimates. Instead of using a uniform set of initial guesses, we can use the single-component prediction fit as a starting point, adopting s/n as the initial guess for s, n components, as well as u and η. Such an approach greatly improves $k = 30$ prediction results, at least when the predicted component is restricted to a small number of n, which is $n = 3$ in this example. Furthermore, decreasing the convergence error tolerance by four orders of magnitude mitigated premature convergence and yielded a visually two-component model (Figure 12c).

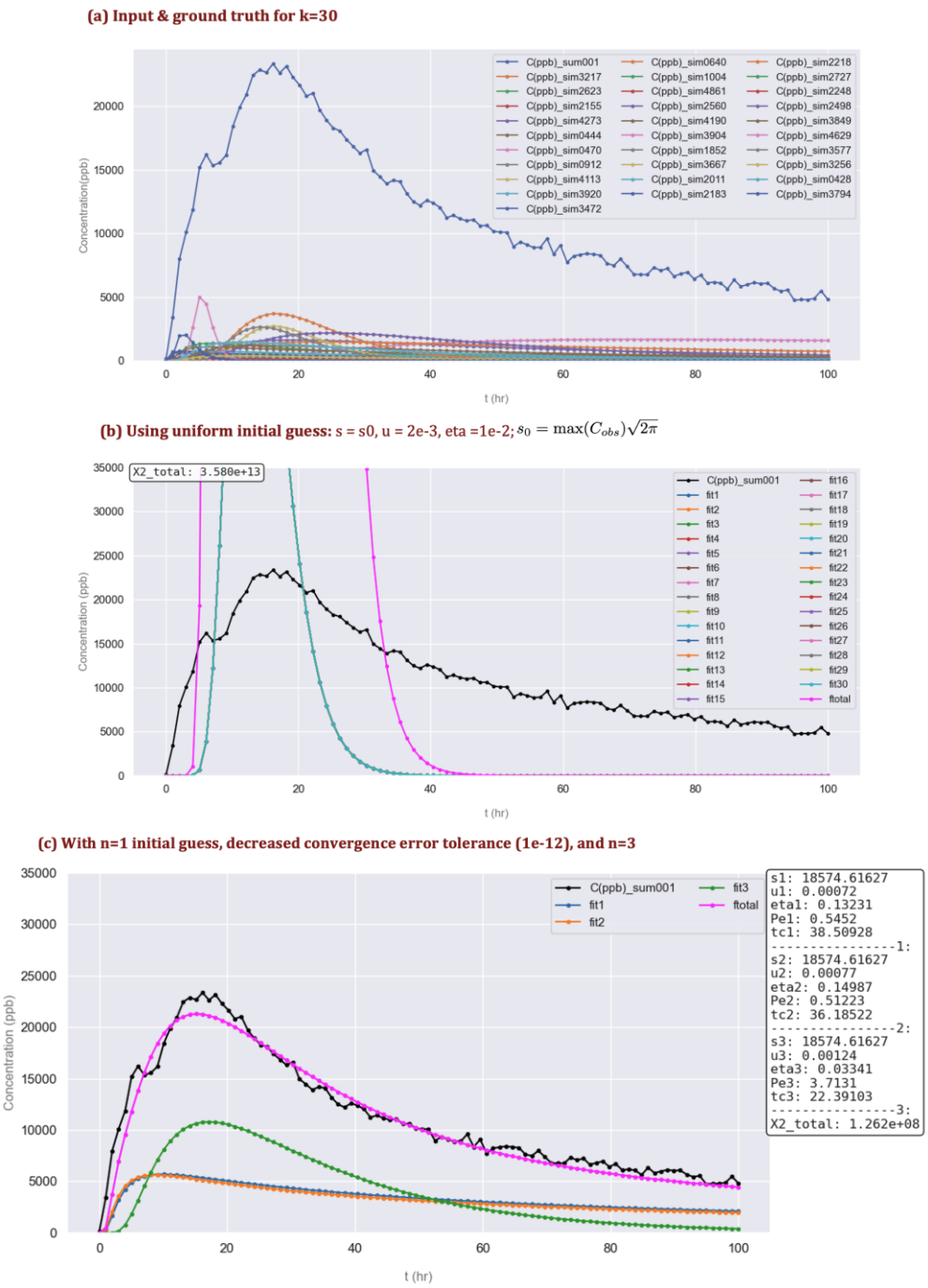

Figure 12: prediction results of k=30 model with (a) uniform initial guesses, (b) the correct parameter values, (c) initial guesses adopted from single-component prediction, and (d) decreased convergence error tolerance of 1e-12.

4. CONCLUSION

The stim tracer analysis encompasses various deployment and sampling strategies, including the use of chemical versus nanotracers, different sampling durations, and sampling frequencies. Inferences regarding flow paths and fracture connectivity depend on understanding the effects of these deployment methodologies and of sample processing on the recorded concentration results. Simultaneously deploying both nano- and chemical stim tracers would help confirm their behavior and effectiveness, as well as establish a baseline for subsequent analyses. Given that the nanotracer dataset consistently showed more erratic patterns than the chemical tracers, it is recommended to supplement nanotracer stimulation with chemical tracers as a control. Additionally, extending the sampling duration to at least 7 days, ideally longer, would allow capturing the full trend of tracer recovery.

The initial attempt at multicomponent tracer modeling in EGS wells demonstrated promising results, especially when involving a few components. Improvements to the modeling techniques will be explored so that the model can sufficiently handle a larger number of

components. Deep learning techniques are also being tested; the resulting decrease in loss function looks promising. Improvements to the architecture, such as adding a penalty to discourage the deep learning model's tendency to take shortcuts in its predictions, will be explored.

ACKNOWLEDGEMENTS

We acknowledge financial support from the U.S. Department of Energy through a subcontract with Fervo Energy, which made this study and research possible.

NOMENCLATURE

q	Flow rate	Cost	cost of matching matrix (i.e., relative L2 norm)
Δt	Delta-time	X	Boolean matrix denoting assignment
s	Mass injected	Y_{true}	Output ground truth
Pe	Peclet number	Y_{pred}	Output prediction
t_c	Mean tracer arrival time (peak arrival time)	$C_{pred}(t, \mathbf{p})$	Predicted concentration at time t given parameters **p** (ppb)
x	Fracture length (m)	$C_{obs}(t)$	Observed concentration data at time t (ppb)
$c_i(t)$	The true monitoring-well concentration at time t as if there were no recycling (ppb)	**p**	Vector of unknown parameters for all components, **p** = $[s_1, u_1, \eta_1, \ldots, s_k, u_k, \eta_k]$ for k input components
$c'_i(t)$	The observed monitoring-well concentration at time t, includes recycling effects (ppb)	$f_{target,\,k}$	Known target mass fraction for component k (m^2/s)
M	Total tracer mass originally injected (g)	*s_frac*	Fraction of $s_1, \ldots s_k$ for k input components
t_1	Time when produced tracer first begins to be recycled into the injector	W	Weighting factor for *s_frac*
$c_1(\tau)$	Tracer concentration in the injection stream at time τ (g/gal)		
$W_1(\tau)$	Injection flow rate at time τ (gal/min)		
$c_i(t-\tau)$	Monitoring well response at lag $(t-\tau)$ to tracer injected at time τ (ppb)		

REFERENCES

De Melo R. C. B., Manohar, M., Shokanov, T., Guo, Q., Oliver, J., Jejelowo, P. (2024). Integration of Ultra-High-Resolution Nano Tracers in Flow Diagnostics with a Multi-Stage Completion Program for Post-Frac Flow Assurance, Fault Evaluation and Well Spacing Optimization in Eagle Ford Shale. In: ADIPEC 2024. SPE, Abu Dhabi, UAE, p D031S120R001

McLennan, J., England, K., & Swearingen, L. (2024). Utah FORGE: Wells 16A(78)-32 and 16B(78)-32 Extended Circulation Test Data - August and September 2024. [Data set]. Geothermal Data Repository. Energy and Geoscience Institute at the University of Utah. https://doi.org/10.15121/2475065Fossum, M.P., and Horne, R. N. (1982). Interpretation of Tracer Return Profiles at Wairakei Geothermal Field Using Fracture Analysis. Geothermal Resources Council (GRC) Transactions Vol 6., October 1982.

Fercho, S., Norbeck, J., Dadi, S., Matson, G., Borrell, J., McConville, E., Webb, S., Bowie, C., Rhodes, G.(2025). Update on the Geology, Temperature, Fracturing, and Resource Potential at the Cape Geothermal Project Informed by Data Acquired from the Drilling of Additional Horizontal EGS Wells. Proceedings 50th Workshop on Geothermal Reservoir Engineering Stanford University, Stanford, California, February 10-12, 2026.

Fredd, C., Cerf, C., Giri, P., Hartvig, S., Huseby, O. (2025). Advanced Tracer Interpretation at Utah FORGE Provides New Insights on Completion and Stimulation Challenges for EGS. Presented at the U.S. Department of Energy GEODE Dissemination Events on January 17, 2025.

Fredd, C., Giri, P., Hartvig, S., Huseby, O., McLennan, J., England, K. (2025). New Insights into Flow Path Characteristics at Utah FORGE Unlock Opportunities for Optimizing Enhanced Geothermal System.GRC Transactions Vol. 49, 2025.

Guo, Q., Oliver, J., & Shokanov, T. (2025). Utah FORGE: QuantumPro Well 16A(78)-32 and 16B(78)-32 Stimulation and Circulation Tracer Test Results - 2024. [Data set]. Geothermal Data Repository. QuantumPro Inc.. https://doi.org/10.15121/2507443

Grant, M.A., and Bixley, P. F. (2011). Geothermal Reservoir Engineering. Elsevier.

Hartvig, S. (n.d.). Restrack Inter-well Tracing Technology. Restrack Inc.

Hartvig, S., Huseby, O., Fredd, C., & Giri, P. (2025). Utah FORGE: RESMAN Well 16A(78)-32 and 16B(78)-32 Stimulation and Circulation Tracer Test Results - 2024. [Data set]. Geothermal Data Repository. RESMAN Energy Technology. https://doi.org/10.15121/2507444

Kim, T., Dunham, E. M., Dadi, S., Segall, P., Gibson, R. L., Titov, A., Chu, S., Norbeck, J., (2025). Evidence of Direct Fluid Connections Between Hydraulic Fractures and Pre-existing Faults at the Cape Station EGS Project. Proceedings 51st Workshop on Geothermal Reservoir Engineering Stanford University, Stanford, California, February 9-11, 2026.

Shook, G. M., Forsmann, J. H. (2005). Systematic Method for Tracer Test Analysis: An Example Using Beowawe Tracer Data. Proceedings, Thirtieth Workshop on Geothermal Reservoir Engineering, Stanford University, Stanford, California. January 31 – February 2, 2005.

Singh, A., Galban, G., McClure, M., Briggs, K., Norbeck, J. (2025). Designing the Record-Breaking Enhanced Geothermal System at Project Cape. In: Proceedings of the 2025 Unconventional Resources Technology Conference. American Association of Petroleum Geologists, Houston, Texas, United States.

Swearingen, L. (2024). Utah FORGE: Wells 16A(78)-32 and 16B(78)-32 Circulation Test Daily Reports from August 2024 . [Data set]. Geothermal Data Repository. Energy and Geoscience Institute at the University of Utah. https://doi.org/10.15121/2455019